MATHEMATICS OF GRAVITATION
PART II, GRAVITATIONAL WAVE DETECTION
BANACH CENTER PUBLICATIONS, VOLUME 41
INSTITUTE OF MATHEMATICS
POLISH ACADEMY OF SCIENCES
WARSZAWA 1997

PULSAR RADIATION

JANUSZ GIL, AGNIESZKA KRAWCZYK

Astronomical Centre, Pedagogical University
Lubuska 2, 65-265 Zielona Góra, Poland
E-mail: jag@astro.ca.wsp.zgora.pl, aga@astro.ca.wsp.zgora.pl

GEORGE MELIKIDZE

Abastumani Astrophysical Observatory
Kazbegi Ave. 2, Tbilisi 380060, Republic of Georgia

Abstract. In this paper we propose a new model of the coherent pulsar radio emission, based on previous work of Ruderman and Sutherland (1975). We assume a non-stationary polar gap braking down via a number of localized spark discharges, feeding a corresponding subpulse-associated plasma columns in the pulsar magnetosphere. Central spark operates at the local pole of the surface magnetic field and other sparks perform more or less ordered circumferential motion around it due to the $E \times B$ drift. We argue that such an arrangement of the polar cap is supported by the observational data. We demonstrate that each spark occupies a region of the polar cap with a characteristic dimension approximately equal to the height of the gap. This is also a typical distance between sparks. The life time of each spark is very short ($\leq 10\mu$s) but they can reappear at approximately the same places due to heating of the surface beneath them by the back-streaming electrons. Thus, the sparks can operate at approximately the same place quite long, alternating between the developing and the terminating phase. The typical time span between two consecutive sparks is less than about 1 μs. We assume that the local surface magnetic field has a complicated multipolar structure with a radius of curvature of field lines smaller than the neutron star radius. Although this is not critical for our model, we further assume that the actual surface field has a sunspot like structure. If this is so, then charged particles accelerated within the high voltage gap region never leave the neutron star surface. This avoids the long standing "current closure" problem. However, the high energy curvature photons produced within the gap during the motion along closed field lines can reach the region above the gap, where the physical conditions are still suitable to produce clouds of secondary plasma due to the Sturrock's multiplication process. Each cloud has a broad energy distribution function. The Lorentz factor γ of a bulk plasma is about 100 but γ of the high energy tail is about few hundreds. The faster particles of the following plasma cloud can overcome the slower bulk particles of

1991 *Mathematics Subject Classification*: Primary 85A45.
The paper is in final form and no version of it will be published elsewhere.

the preceding one, acting as a beam penetrating plasma. This ignites a typical beam-plasma instability generating well known electrostatic Langmuir waves. Detailed calculations show that the amplitude of these waves is high enough to cause a non-linear evolution, leading to soliton formation. The net charge of a relativistically moving soliton is a source of the coherent curvature radiation powerful enough to explain observed pulsar luminosities. It is worth emphasizing that, for the first time, this is a self-consistent model of pulsar radiation. The coherent curvature radio emission by solitons in our model is a consequence of a putative existence of a non-stationary polar gap braking down via exponentially developing sparks.

1. Introduction. Although almost 30 years have past since discovery of pulsars, their radiation still remains mystery. This concerns both the fundamental problem of the coherent radio emission as well as the specific modulation of pulsar radiation in the form of individual pulses and the characteristic stable mean profiles. Ruderman and collaborators in a series of papers (Ruderman and Sutherland 1975, Cheng and Ruderman 1977, 1980) have proposed an attractive theory of pulsars. They attempted to solve for both the mechanism of coherence of single particle radiation as well as the organization of emitting regions. Although their two-stream plasma instability has proven inefficient in producing observable radio emission, the latter was partially successful in explaining details of pulsar radiation modulation. The major feature of their pulsar picture is the non-stationary polar gap above the polar cap, braking down via a number of isolated spark discharges. The sparks develop wherever the gap potential drop is above the threshold for the electron-positron pair production in the strong pulsar magnetic field, populating the polar cap as densely as possible. These sparks feed a corresponding subpulse-associated plasma columns in the pulsar magnetosphere, where the pulsar radio emission originates. From the phenomenological point of view this picture seems to be supported by observational data (Gil and Krawczyk 1996a, Gil et al. 1995). Problems arise when one tries to understand an underlying physics. The existence of the polar gap has been criticized on the grounds of quantum-mechanical calculation of the binding energy on the neutron star surface. It has been shown that the work function is too small for the polar gap to form. However, recently Björnsson (1996) argued that the short time scale variability of the global current distribution could prevent a steady flow of charged particles from the pulsar surface, even for negligible binding energy. As a result, a situation similar to that delineated by Ruderman and Sutherland (1975, hereafter RS) may arise. In this paper we propose a pulsar model based on a putative existence of non-stationary polar gap.

The properties of the curvature radiation explain most naturally the complex polarization characteristic of individual as well as average pulse profiles (Gil and Snakowski 1990a, b; Gil 1992, Gil et al. 1993a, Gil and Lyne 1995). The smooth variations of the average position angle curve are very consistent with the Rotating Vector Model (Radhakrishnan and Cooke 1969, Manchester and Taylor 1977; henceforth RVM), in which the mean pulsar radiation is polarized in direction either parallel or perpendicular to the planes of axially symmetric (dipolar) magnetic field, with the axis of symmetry coinciding with the beam axis. This geometrical model applies to a variety of physical radiation mechanisms, including the curvature radiation. Blaskiewicz et al. (1991) generalized the RVM model to include the special relativistic correction due to fast corotation, which

apply exclusively to the curvature radiation. They argued that the particle acceleration follows not only from the curvature of field lines but also from the corotational motion. The relativistic corrections are easily detectable and they have been found in a number of bright pulsars (Blaskiewicz et al. 1991, Gil and Krawczyk 1996b). The clear demonstration of relativistic effects modifying the curvature acceleration by corotational component is the most convincing argument supporting the mechanism of coherent curvature radiation as the actual source of pulsar radio emission. In this paper we propose a new, self-consistent pulsar model based on plasma physics and properties of curvature radiation.

2. Polar gap, sparks and structure of the pulsar beam. Sparks as primary sources of the subpulse associated plasma columns have also been criticized, mostly due to short dynamical times scales (~ 10 μs) as compared with the subpulse time scales. We propose a modification of the sparking model in a following way: the most intense sparking discharge occurs at the local surface magnetic pole ([1]), where the magnetic field is strongest. The life-time of this spark, that is the period needed to develop the corotational charge density within the gap volume occupied by the spark, is very short ($\leq 10\mu$s). However, the polar cap surface beneath the spark is heated up to X-ray temperatures by the back streaming electrons, which ignites an intense thermo-emission. These seed charged particles should cause reappearance of the spark after short time at approximately the same place. Therefore, an oscillating sparking discharge should be active on the local surface magnetic pole for a long time, comparable with the subpulse time scales. The same should occur at any other part of the polar cap area where the gap potential drop is above the threshold for electron-positron pair creation.

2.1. *Spark characteristic dimension.* From the width of subpulses interpreted as plasma columns fed by sparks (RS) one can estimate the fraction $f = (D/r_p)^2$ of the polar cap area filled by spark in the range 10^{-1} to 10^{-2}, where D is a characteristic spark dimension and $r_p = 1.45 \cdot 10^4 P^{-1/2}$ cm is the polar cap radius defined by the dipolar component of the pulsar magnetic field[1]. As argued by the RS, each spark inhibits formation of another spark within a distance approximately equal to the polar gap height

$$h = 5 \cdot 10^3 \mathcal{R}_6^{2/7} P^{3/7} B_{12}^{-4/7} \quad [\mathrm{cm}], \tag{1}$$

where $B_{12} = B_s/10^{12}\mathrm{G} \approx 3.9 \cdot 10^7 (P \cdot \dot{P})^{1/2}$ and $\mathcal{R}_6 = \mathcal{R}/10^6$ cm is the radius of curvature of the surface magnetic field[1] in units of 10^6 cm. One can form a dimensionless parameter

$$a \approx \frac{r_p}{h} = \frac{5 \cdot 10^4}{\mathcal{R}_6^{2/7}} \dot{P}^{2/7} P^{-9/14}, \tag{2}$$

([1]) It is assumed that the local surface magnetic field has a sunspot like structure with the radius of curvature $\mathcal{R} \leq 10^6$ cm. It seems that there exist both theoretical (Ruderman 1991 a,b,c) and observational (Page and Sarmiento 1996, Bulik et al. 1992) support for such a structure of surface magnetic field. The strength of this multipolar magnetic field should be comparable with the surface value of the global dipole pulsar magnetic field. Thus, the polar cap radius r_p is determined by the Goldreich-Julian value, at least in typical pulsars.

describing the ratio of polar cap to spark dimensions. For a typical pulsar with $P = 0.6$ s, $\dot{P} = 10^{-15}$ and $\mathcal{R}_6^{2/7} \approx 1$ the Eq. 2 gives $h \approx 0.3\, r_p$. On the other hand $D/r_p = f^{1/2} \approx 0.3$ or $D \approx 0.3\, r_p$. By comparison one can conclude that the characteristic spark dimension is approximately equal to the RS gap height $D \approx h$ (Eq. 1).

One can estimate the spark dimension using an independent physical arguments. The number density of the $e^- e^+$ pairs in the sparking avalanche should develop exponentially with time

$$n \approx n_{GJ} e^{-\tau/t}, \tag{3}$$

where n_{GJ} is the Goldreich-Julian (1969) number density, t is the time and τ is the exponentiation time scale, describing a time interval after which the spark charge density reaches the corotational value screening the gap. Let us notice that the exponentiation time scale τ should be inversely proportional to the radius of curvature $\mathcal{R}$ of the surface magnetic field. In fact, a copious pair production within the gap requires large perpendicular component of the magnetic field $B_\perp \sim hB/\mathcal{R}$. For a given B, the curvature photon has to travel a distance $l \leq h$ to reach the value of $B_\perp$ high enough to produce a pair. The smaller the radius of curvature $\mathcal{R}$, the smaller the distance l. Thus, $\tau \propto 1/B_\perp$ and a natural spark exponentiation time scale is

$$\tau \approx \mathcal{R}/c. \tag{4}$$

For small radius of curvature[1] $\mathcal{R} \approx 3 \cdot 10^5$ cm this is about 10 μs, which is equal to the value obtained by independent argument in RS (1975).

If the surface magnetic field has a sunspot like structure[1], then there should exist a quasi-axial symmetry of the planes of field lines centered on the local pole (generally not coinciding with the global dipole axis). First, let us consider a spark developing near the local pole. In a curved magnetic field the spark plasma is subject to drift motion towards the pole with a speed

$$v_\parallel \approx ch/\mathcal{R}, \tag{5}$$

(Cheng and Ruderman 1977, 1980). Thus, during the time τ (Eq. 4), the spark will cover a distance $\mathcal{D} \approx v_\parallel \cdot \tau \approx (hc/\mathcal{R})(\mathcal{R}/c) = h$ moving towards the pole. Another drift motion to be taken into account is the well known $E \times B$ drift, which causes circulation of the plasma around the pole. The maximum speed of this drift corresponds to empty gap and can be expressed by

$$v_\perp \approx c\Delta E/B, \tag{6}$$

where ΔE is the gap component of pulsar electric field (RS). Since the velocities $v_\parallel$ and $v_\perp$ are comparable, they will both cause the spread of initially plane spark to a two dimensional entity with a characteristic dimension h. The same arguments apply to non-central sparks. One should consider both drift motions, parallel and perpendicular to the field line planes (Eqs. 5 and 6), and notice that the existence of the central spark will prevent to some extent the drift along the planes of drift lines toward the pole. In fact, sparks have to be separated from each other by about h and quasi-stable position of the central spark on the local pole determines range of distances from the pole that can be occupied by other sparks. On the other hand, the perpendicular $E \times B$ drift will cause the spread of spark plasma across the planes of field lines. As a result both drift

motion will cause spreading of initially small and plane discharge into a two-dimensional entity of diameter

$$\mathcal{D} \approx h, \tag{7}$$

which means that a characteristic spark dimension is approximately equal to the RS polar gap height (Eq. 1).

2.2. *Spark dynamics.* When the initial electron-positron pair is produced, it experiences the full polar gap potential drop $\Delta V_{max} = 2\pi B_s h^2/cP$ (RS), where $B_s \approx B_{12} \cdot 10^{12}$ G is the surface magnetic field, and h is the height of the polar gap (Eq. 1) determined by the mean free path for the photon pair production in the strong pulsar magnetic field (Erber 1966, RS 1975). Assuming that B_s is comparable with the surface value of the global dipole field $B_d = 3.2 \cdot 10^{19}(P\dot{P})^{1/2}$ G, the maximum potential drop in the polar gap can be written as

$$\Delta V_{max} = 5.2 \cdot 10^9 B_{12}^{-1/7} P^{-1/7} \mathcal{R}_6^{4/7} \ [\mathrm{g}^{1/2}\mathrm{cm}^{1/2}\mathrm{s}^{-1}] = 1.7 \cdot 10^{12} \mathcal{R}_6^{4/7} B_{12}^{-1/7} P^{-1/7} \ [V]. \tag{8}$$

The electron and positron are accelerated to relativistic velocities in the opposite directions within the polar gap. Since the relativistic motion along curved magnetic field lines ($\mathcal{R}_6 \leq 1$)[1], they emit high frequency curvature photons which are able to produce additional pairs on adjacent field lines as long as $\hbar\omega > 2m_e c^2$, where m_e is the electron mass and $\omega \approx \gamma^3 c/\mathcal{R}$ (here $\hbar$ is the Planck constant). The positron leaves the gap acceleration region with the maximum Lorentz factor

$$\gamma_{max} = \frac{e\Delta V_{max}}{m_e c^2} = 3.4 \cdot 10^6 \mathcal{R}_6^{4/7} B_{12}^{-1/7} P^{-1/7}. \tag{9}$$

On the other hand, the electron hits the polar cap and deposits its kinetic energy just beneath the surface. This will result in the thermal X-ray emission and/or thermionic emission of charged particle(s), which will cause discharge exponentiation along the original field line. As argued in section 2.1 this initial discharge will spread rapidly during the exponentiation time $\tau \approx \mathcal{R}/c$ into a two-dimensional entity, with the characteristic dimension $\mathcal{D} \approx h$ (Eq. 1). The polar gap is filled with a number of isolated flux tubes with exponentially growing density, called sparks. Their characteristic dimensions as well as typical distances between them are approximately equal to the RS gap height (Eq. 1).

At the beginning of the sparking discharge $t \ll \mathcal{R}/c$ and $n \ll n_{GJ} = B_s/(\pi^2 Pce)$. During most of the exponentiation time $\tau \approx \mathcal{R}/c$ (Eq. 4) $n < n_{GJ}$ (Eq. 3). At this stage the spark delivers to the magnetosphere above the polar cap a column of low density $n < n_{GJ}$ and high energy positrons with the Lorentz factor $\gamma \approx 3 \cdot 10^6 \mathcal{R}_6^{4/7}$ (Eq. 9). These high energy positrons form a secondary electron-positron plasma via the Sturrock multiplication process (Sturrock 1971, RS). And in the final stage of sparking discharge when $t \approx \mathcal{R}/c$ and $n \approx n_{GJ}$, the maximum potential drop (Eq. 8) is rapidly reduced to the value slightly below the threshold for the copious pair production

$$\Delta V_{min} = \gamma_{min} m_e c^2/e, \tag{10}$$

where $\gamma_{min} = (2m_e c^2 \mathcal{R}/c\hbar)^{1/3}$ or

$$\gamma_{min} \approx 3.3 \mathcal{R}_6^{1/3} \cdot 10^5. \tag{11}$$

From Eqs. (10 and 11) it follows that the sparking discharge terminates (after $\tau \approx \mathcal{R}/c \sim$ few microseconds) when the potential drop decreases by the factor

$$\mathcal{F} = \frac{\Delta V_{min}}{\Delta V_{max}} \approx 0.108 \cdot \mathcal{R}_6^{-5/21} B_{12}^{1/7} P^{1/7} \approx 0.1 \mathcal{R}_6^{-5/21}. \tag{12}$$

When this stage is reached, the spark delivers for a short time $\Delta t \approx h/c$ a beam of high density ($n \approx n_{_{GJ}}$) monoenergetic positrons with a low Lorentz factor γ determined by Eq. 11. We will call this stage the "spark-emptying" or "gap-emptying" phase. During this phase the $E \times B$ drift velocity (Eq. 6) is also reduced by the filling factor $\mathcal{F}$ (Eq. 12). Thus, the initially plane discharge expands rapidly with the maximum velocity $v \approx ch/\mathcal{R} \approx c\Delta E/B$ (Eqs. 5 and 6) during $\tau \sim \mathcal{R}/c$, but a fully developed beam of high density $n = n_{_{GJ}}$ positrons drifts with much lower velocity

$$v_d = c\mathcal{F}\Delta E/B_s \text{ [cm/s]}, \tag{13}$$

where ΔE is the gap component of the electric field near the pulsar cap surface (RS). This could explain the slow subpulse drift observed in some pulsars, provided that the spark can reappear at approximately the same place, modulo the $E \times B$ drift with velocity v_d (Eq. 13). This however is a natural property of the sparking discharge. In fact, due to the slow drift in the gap-emptying phase, the back side edge of the spark (with respect to the direction of $E \times B$ motion) will still feel the potential drop slightly above the pair production threshold value (Eqs. 10 and 11). Thus, the seed thermionic particles can restart exponentiation at the back side of terminating spark, which will then expand rapidly (in the direction of $E \times B$ drift) with the fast drift velocity corresponding to the empty gap (Eq. 6). Then again a fully developed spark (and a corresponding subpulse-associated plasma column above this spark) will drift with a slow velocity described by Eq. 13 (see section 4).

2.3. *Polar cap structure.* As argued in previous sections, the polar cap should be populated by a number of sparks of diameter $D \approx h$ (Eq. 7), separated from each other also by about h (Eq. 1). The strongest spark (core) is operating on the local magnetic pole and other sparks (conal) circulate around the polar one due to $E \times B$ drift phenomenon (RS). This leads to the ring structure of the polar cap and in consequence to the core/conal structure of the average pulsar beam (Rankin 1983, 1990, 1992, 1993; Gil and Krawczyk 1996a). A number of cones surrounding the central, quasi-stationary "core" beam associated with the polar spark is determined by the ratio

$$n = \frac{1}{2}a \approx 2.5 \cdot 10^4 \cdot \mathcal{R}_6^{-2/7} \cdot \dot{P}^{2/7} \cdot P^{-9/14}. \tag{14}$$

The number of actual profile components is

$$N \leq N_{max} = a + 1, \tag{15}$$

depending on the impact angle of the closest approach of the observer to the magnetic axis, where the equality corresponds to the case when the observer's line-of-sight passes close to the magnetic axis.

Whithin the above scenario one can expect that for a complex profiles of types cT (conal Triple), Q (Quadruple) and M (Multiple) the value of a should be about 4 (two

cones), which according to Eq. 2 means that $5 \cdot 10^4 \dot{P}^{4/14} P^{-9/14} = 4 \cdot \mathcal{R}_6^{2/7}$. Thus, the cT, Q and M profiles should follow a definite slope

$$\dot{P} = 5 \cdot 10^{-15} \mathcal{R}_6 P^{2.25} \tag{16}$$

on the $P - \dot{P}$ diagram. As one can see from Fig. 1, this is apparently so.

Pulsars marked with ($\times$) corresponding to the complex profiles (cT, Q and M) follow the slope expressed in Eq. 16, where the adopted value of $\mathcal{R}_6 = 1., 0.1, 0.01$ is marked on the right side of a dead line. It is worth noting that the slope predicted by the RS (Eqs. 2 and 16) extends over four orders of magnitude in P and at least nine orders of magnitude in $\dot{P}$.

The parameter $a = r_p/h$ describing the ratio of polar cap to spark dimensions covers the range $2 < a < 200$ (assuming $\mathcal{R}_6^{-2/7} \approx 1$ in Eq. 2). Generally, the $P - \dot{P}$ relationship following from Eq. 2 is

$$\dot{P} = 3.6 \cdot 10^{-17} \mathcal{R}_6 \cdot a^{3.5} P^{2.25}. \tag{17}$$

For $a = 4$ the Eq. 17 reduces to the Eq. 16 describing slopes presented in Fig. 1. The actual value of a is reflected by the size of the circle. Both the pulsars with complex profiles (marked by $\times$) and those with drifting subpulses (marked by $+$) occupy the region of small $a < 10$. On the other hand pulsars with large values of $a > 10$ should have simple, amorphous profiles with no hints of subpulses in single pulses. The large number of small sparks will correspond to the microstructure rather than to subpulses in such cases. The stars within the circles indicate pulsars with amorphous and simple profiles. These pulsars demonstrate unuasually high degree of linear polarization (Gould 1994), which we believe is also a consequence of large value of a (Gil et al. 1996).

The structure of the $P - \dot{P}$ diagram presented in Fig. 1 strongly supports the idea of subpulse-associated sparks drifting circumferentialy around the local surface magnetic pole on the polar cap. The natural interpretation of Fig. 1 is that the sparks do exist on the Goldreich-Julian (1969) polar cap and they determine the morphology of the mean pulsar profiles. Indeed, the complexity of the profile and appearance of drifting subpulses increases with decreasing parameter a (size of the circle). Moreover, the complex profile pulsars (cT, Q, M) as well as pulsars showing drifting subpulses follow the slope which can be derived from the RS model (Eqs. 1 and 2). The stability of mean profiles as well as drifting subpulse patterns is a consequence of permanent sparking activity on the local surface magnetic pole, which restricts the degrees of freedom of spark motion to a circumferential movement around the pole.

3. Coherent pulsar radio emission. From the observational evidence presented in section 2 it follows that the coherent pulsar radiation originates within the subpulse-associated plasma columns developed by sparks operating on the polar cap. Most probably this is a coherent curvature radiation originating at altitudes lower than about 10% of the light cylinder radius $R_L = cP/2\pi$ (Blaskiewicz et al. 1991). To examine the structure of the electron-positron plasma in the subpulse-associated column we have to take into account the spark dynamics discussed in sections 2.1 and 2.3. Although we will concentrate on the dynamics of just one spark, we keep in mind that the polar cap is

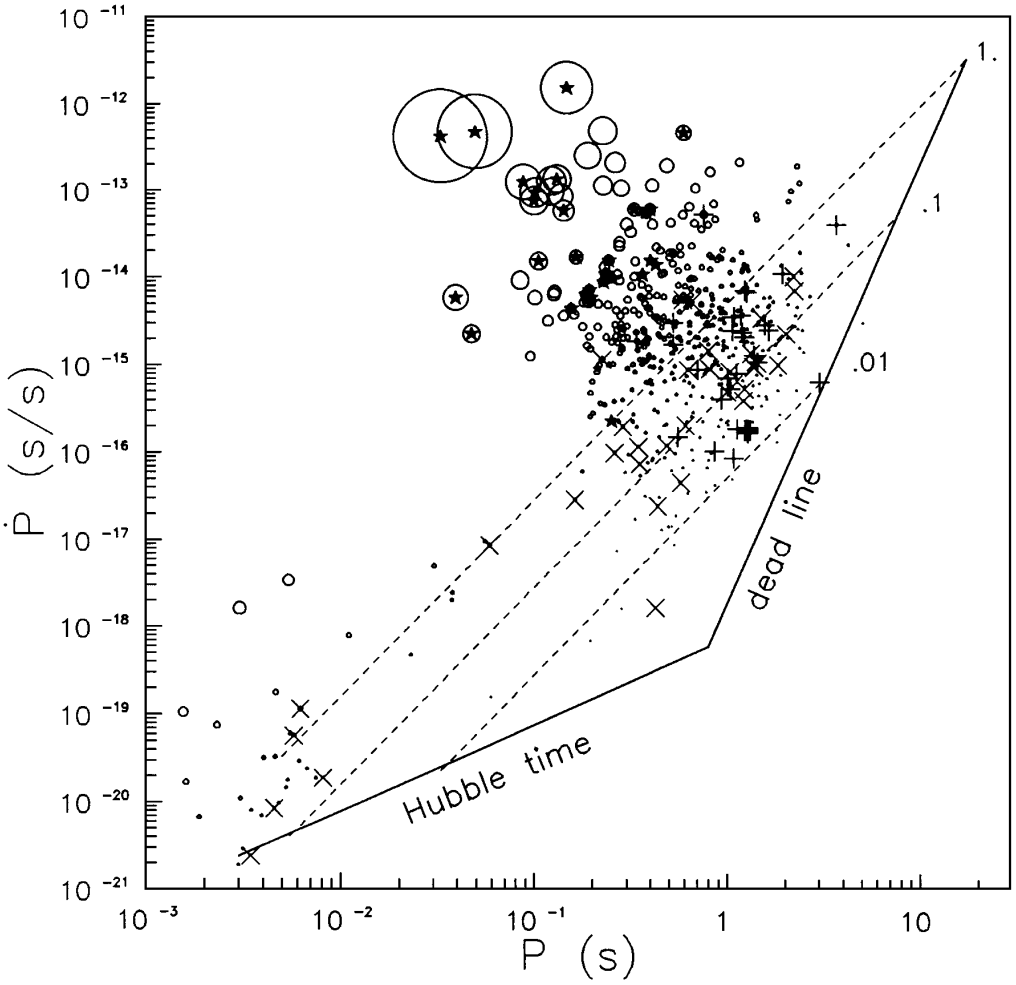

Fig. 1. $P - \dot{P}$ diagram for 600 known pulsars. The value of the parameter $a = r_p/h$ is marked by the size of the circle (largest corresponding to the Crab pulsar with $a \approx 200$ and smallest corresponding to $a \approx 2$). Pulsars marked additionally by ($\times$) correspond to stars with complex cT, Q and M profiles, for which $a \approx 4$. Those marked additionally by (+) show drifting subpulses (thick cross corresponds to the case of PSR 0809+74). The star within a circle indicate simple, amorphous profiles. Three dashed lines describe the slopes corresponding to the values of $\mathcal{R}_6 = 1$, 0.1 and 0.01, respectively (calculated for $a = 4$, i.e. $\dot{P} = 5 \cdot 10^{-15} \mathcal{R}_6 P^{2.25}$). The Hubble time and dead line limits correspond to $P/\dot{P} = const$ and $\dot{P}/P^5 = const$ relationships, respectively.

populated with a number of sparks as densely as possible, i.e. they develop wherever the gap potential drop is above the threshold for the copious pair creation (Eq. 10). The characteristic dimension of sparks as well as typical distance between them is about the polar gap height (Eq. 1).

3.1. *Linear theory.* The properties of the secondary electron-positron plasma created via the Sturrock's multiplication process by the primary positrons with $\gamma = \gamma_{max}$ depend on the radius of curvature $\mathcal{R}$ of magnetic field lines above the gap, where the accelerating electric field is negligible. Since we assumed $\mathcal{R} \leq 10^6$ cm, then the Sturrock multiplication factor $\chi \approx 10^4$ and the Lorentz factor of the secondary plasma $\gamma_p \approx 100$ (Gil et al. 1996). This secondary plasma with a number density $n_p = \chi_p \cdot n_{_{GJ}}$ is penetrated by the beam of plasma particles with $\gamma_b \leq \gamma_{min}$ (Eq. 11) from the high energy tail of the distribution function of the secondary plasma cloud associated with very next spark. This should lead to instabilities which can be crucial for generating the coherent pulsar radio emission.

Let us consider a secondary electron-positron plasma with density $n_p = \chi_p \cdot n_{_{GJ}}$ and Lorentz factor $\gamma_p \approx 100$ penetrated by the beam with density $n_b = \chi_b \cdot n_{_{GJ}} < \chi_p n_{GJ}$ and Lorentz factor $\gamma_b \leq \gamma_{min}$ (Eq. 11). The stability of such plasma against the beam penetration has been examined by several authors (RS, Benford and Buschauer 1977, Asséo et al. 1980, 1983, Egorenkov et al. 1983). A number of instabilities have been found but none of them has proven applicable to pulsar radio emission (e.g. Melrose 1995). Here we will propose a new possibility, which is a consequence of non-stationary gap discharged by a number of sparks, discussed in sections 2.1, 2.2 and 2.3.

It is well known that the strong Langmuir turbulence will develop in the secondary plasma due to the beam-plasma instability caused by resonant interaction of the beam and plasma particles (Krall and Tripolpiece 1973). We believe that the role of the beam is played by the faster particles of the secondary plasma produced by the primary beam associated with the very next spark ($n_b < \chi_p n_{_{GJ}}$ and $100 < \gamma_b < \gamma_{min}$). At the linear stage the necessary condition for development of the Langmuir wave can be written as (Egorenkov et al. 1983, Usov 1987)

$$\frac{r}{R} \ll 500 \cdot B_{12} \cdot P^{-1} \cdot \chi_b^{2/3} \cdot \left(\frac{\chi_p}{10^4}\right)^{1/3} \cdot \left(\frac{\gamma_b}{10^4}\right)^{-2} \cdot \left(\frac{\gamma_p}{10^2}\right)^{-1}, \tag{18}$$

where r is an altitude and $R \simeq 10^6$ cm is the neutron star radius. It follows from the above condition that if $\gamma_b \ll 10^6$ then $r/R < 50$. This is obviously possible in our non-stationary model where $\gamma_b \leq \gamma_{min} \leq 10^4$ (Eq. 11), but it would be impossible in the stationary gap model (Arons 1981, 1992), where $\gamma_b \geq 10^6$. It is worth emphasizing that there is no other instability that can develop in the secondary pulsar plasma at altitudes below 10% of the light cylinder radius. Investigations of possible linear effects in pulsar plasma can be found in a number of papers (Lominadze et al. 1986, , Machabeli 1991, Kazbegi et al. 1988,1992 and references therein). Some attractive phenomena like the drift driven and cyclotron instabilities have been found but unfortunately they can only develop at much higher altitudes than $100 \cdot R$, contrary to the observational evidence that $r < 0.1 R_L$ (e.g. Cordes 1992).

As we argued in section 2.2, the two secondary plasma clouds corresponding to the two consecutive sparks are separated by about $\Delta t = h/c$ (typically 10^{-7} s). Let us estimate the time ΔT after which the faster positron beam with $\gamma_b \approx \gamma_{min}$ will overcome the slower secondary plasma with $\gamma_p \approx 100 \ll \gamma_b$. The corresponding velocity difference is determined by the lower Lorentz factor $\Delta v = c/2\gamma_p^2$. It is easy to show that $\Delta T \sim h/\Delta v = 2\gamma_p^2 h/c$, where $h = 5 \cdot 10^3 \mathcal{R}_6^{2/7} B_{12}^{-4/7} P^{3/7}$ [cm]. The distance covered during this

time $\Delta r \sim c\Delta T = 2\gamma_p^2 c \approx 10^2 R\gamma_p^2 \mathcal{R}_6^{2/7} B_{12}^{-4/7} P^{3/7}$. Since $\Delta r \ll R = 10^6$ cm, one can write the expression

$$\frac{r}{R} \sim 10^2 (\gamma_p/100)^2 \mathcal{R}_6^{2/7} B_{12}^{-4/7} P^{3/7}. \tag{19}$$

This is a kinematic estimate of the emission altitude (beam-plasma instability region) which agrees very well with the physical condition expressed by Eq. 18. For the typical pulsar parameter $r \sim 50R$, as expected (see section 4 for the case of the PSR 0809+74). One should realize that B_{12} in Eq. 19 is in fact the surface magnetic field expressed in units of 10^{12} G. Although its strength should be comparable with the dipole component of pulsar magnetic field at the surface, the dependencies on P and $\dot{P}$ could be completely different from $\propto (P \cdot \dot{P})^{1/2}$.

3.2. *The non-linear theory.* The Langmuir waves generated by the beam-plasma instability are just electrostatic oscillations and they cannot leave the plasma without transformation into an electromagnetic wave. The frequency of Langmuir oscillations ω_l is of the order of 100 GHz and therefore the pulsar radio-frequencies $\omega < 100$ GHz cannot be attributed to these oscillations. In fact, the time scale of the process by which the Langmuir bunch radiates, should be shorter than one oscillation period, that is $\omega_l < \omega_c \sim 10^{10}$ s^{-1}. In what follows we will argue that the non-linear evolution of Langmuir waves lead to the formation of stable Langmuir soliton, which radiates coherent radio emission by means of the curvature radiation. Here we will just outline the main results and apply them to the pulsar radio emission.

A packet of plasma waves propagating in the relativistic electron-positron plasma with phase velocities close to (but less than) the velocity of light is modulationaly unstable, and its nonlinear evolution results in the formation of a nonlinear solitary wave solution. This process is described by a nonlinear Schrödinger equation taking into account the nonlinear Landau damping. The role of the low-frequency perturbations in the case of the electron-positron plasma (in the absence of the ion sonic waves) is played by the nonlinear beatings of the plasma waves and the nonlinear dumping is determined by the resonant interaction of the beatings with particles.

The soliton causes the charge separation due the relative motion of electrons and positrons. The charge separation is supported by the ponderomotive force. This kind of charge separation is well known in the laboratory electron-ion plasma (Galeev and Sagdeev 1973, Ichikawa et al. 1973, Karpman et al. 1975). In the electron-positron plasma the net charge is zero due to the mass equality. But if there is some difference in the unperturbed distribution function of electrons and positrons then the net charge of the soliton can be described (in the plasma rest frame) by the following equation

$$\rho \sim \frac{5}{\omega_l^2} \left(\frac{e}{m}\right) \left(\frac{v_o}{c}\right) \frac{E_m^2}{\Delta^2} \frac{3 - 2\cosh^2 b}{\cosh^4 b} \tag{20}$$

(Melikidze and Pataraya 1984), where $b = (x - v_{gr}t)/\Delta$, Δ is the characteristic longitudinal dimension of the soliton and v_o is a relative, macroscopic difference of electrons and positrons velocity, v_{gr} is the group velocity, ω_l is the frequency and E is the amplitude of Langmuir waves, respectively. The qualitative behavior of the soliton charge density is shown in Fig. 2, where the x-axis is calibrated in units of $\frac{1}{2}\Delta$ and the y-axis corresponds

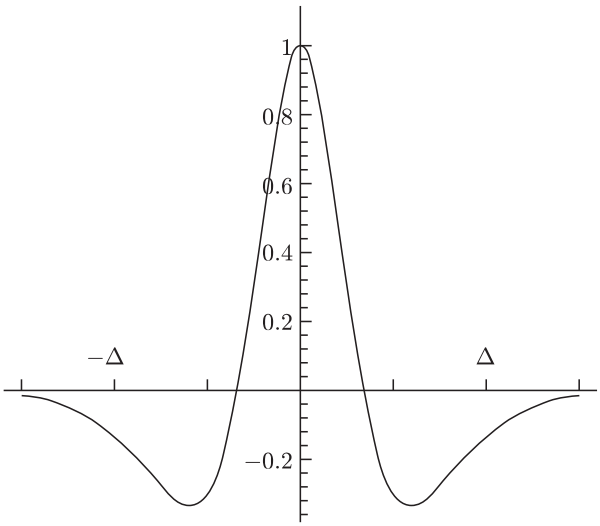

Fig. 2. Schematic representation of the soliton net charge.

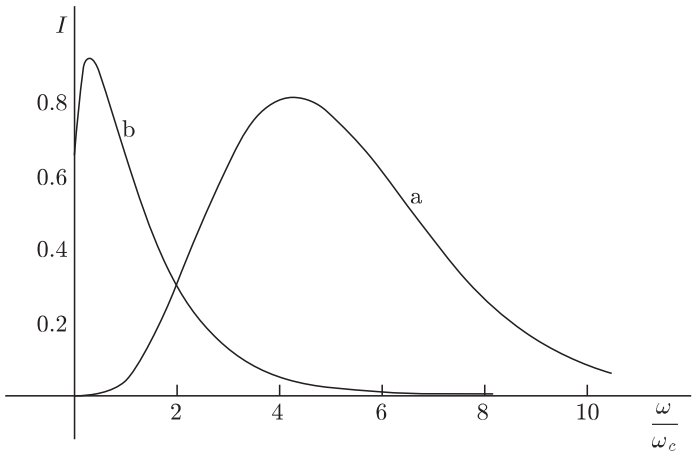

Fig. 3. Spectra of the curvature radiation of the soliton (a), as compared with spectra of the curvature radiation of the small fictitious bunch (b) with the same parameters $(\mathcal{R}, \gamma, Q)$. The vertical scale of the soliton spectrum (a) is expanded by a factor of 500 with respect to (b).

to the net charge. As one can see the soliton is in fact a system of three charges coupled to each other. The time evolution of such system remains to be examined but it is already obvious that the soliton can emit a coherent curvature radiation for a finite time. If one considers the relativistic motion of the soliton along dipolar magnetic field lines with a radius of curvature $\mathcal{R} \sim 10^8$ cm, the spectral power of the curvature radiation is expressed by the equation

$$I_\omega \sim \frac{Q^2}{\mathcal{R}} F\left(\frac{\omega}{\omega_c}\right)\left[1 - \cos\left(a\frac{\omega}{\omega_c}\right)\right]^2 \tag{21}$$

(Melikidze and Pataraya 1984), where Q is the soliton net charge,

$$F(\xi) = \xi \int_{\xi}^{\infty} K_{5/3}(\xi) d\xi, \; a = \frac{3}{2}\gamma_b^3 \frac{\Delta}{\mathcal{R}} \text{ and } \omega_c = \frac{3}{2}\frac{c}{\mathcal{R}}\gamma_b^3.$$

Figure 3 presents the spectra of the soliton curvature radiation calculated from the above equations, as compared with the spectra of curvature radiation of a fictitious bunch with the same charge Q. The maximum intensity of soliton curvature radiation, corresponds to slightly higher frequencies ($\omega/\omega_c \sim 5$) than in the case of single bunch ($\omega/\omega_c \sim 1$). For a typical pulsar parameters these frequencies fall into the radio-band. Preliminary calculations show that the power radiated by solitons that can be generated by the beam-plasma instability is high enough to explain the observed pulsar luminosity. The energy of the soliton curvature radiation is supported by kinetic energy of the secondary plasma created by the primary beam with $\gamma = \gamma_{max}$ (Eq. 9).

The soliton curvature radiation is about 100 times less efficient than the corresponding curvature radiation of a fictitious bunch with the same charge. In fact, the power radiated in the unit frequency range is lower by the factor of 500 but the frequency ω at which the radiation maximum occurs is higher by the factor of 5. It is worth noting that the vertical scale of the soliton spectrum is expanded by a factor 500 in Fig. 3. To estimate the luminosity of pulsar radiation let us first consider the curvature radiation of a fictitious bunch. In order to calculate the bunch net charge we will use the spark model (section 2.1 and 2.2), according to which $Q = eNh^2\lambda$, where N is a number charge density within the bunch , h is the spark height (Eq. 1) and $\lambda < 100$ cm is the wavelength of the emitted coherent radiation. If we assume that only a tiny fraction of secondary plasma with number density $n_{_{GJ}} = n/\chi_p$ is bunched (i.e. density contrast $\delta n/n = 1/\gamma_p < 10^{-4}$), then $N = n_{_{GJ}} = 7 \cdot 10^{10} P^{-1} B_{12}$ [cm^{-3}]. Thus, the power radiated by a fictitious bunch with charge Q is $\mathcal{P}_b \approx Q^2 c\gamma^4/\mathcal{R}^2 \leq n_{_{GJ}}^2 h^4 \lambda^2 \cdot 10^{-16} \gamma_2^4/\mathcal{R}_8^2$ [erg/s], where $(\gamma_p/100) < \gamma_2 = (\gamma/100) > 1$ is the Lorentz factor of fast resonant particles and $1 < \mathcal{R}_8 = \mathcal{R}/10^8$ cm is the radius of curvature of dipolar magnetic field lines in the radio emission region (in units of 10^8 cm). For a typical pulsar $h \sim 10^3$ cm and $B_{12}/P \sim 1$. Taking $\gamma \sim 3$ and $\mathcal{R}_8 \sim 1$ one obtains $P_b \leq 10^{24}$ erg/s, which for approximately 100 times less powerful soliton gives $P_s \leq 10^{22}$ erg/s. For a typical spark exponentiation time $\tau \approx 10$ μs (Eq. 4) one gets $\mathcal{N} \sim 10^5$ sparks per second. Since at the any instant there is $\mathcal{M} \sim 10$ sparks on the polar cap, the luminosity of a typical pulsar

$$\mathcal{L} = \mathcal{P}_s \cdot \mathcal{N} \cdot \mathcal{M} \tag{22}$$

should be smaller than about 10^{28} erg/s. The soliton curvature radiation is powerful enough to explain the observed pulsar luminosities in the range $10^{23} - 10^{28}$ erg/s.

Thus, our radiation model, which is a natural consequence of a non-stationary gap model (sections 2.1, 2.2 and 2.3) agrees with observations well, at least from the energetical point of view. Moreover, it is obvious that the polarization properties of the soliton radiation will be similar to that of the single-particle curvature radiation, which was shown to be consistent with the pulsar polarization characteristics (Gil et al. 1995, Gil and Lyne 1995, Gil and Snakowski 1990, Gil et al. 1993b).

4. Drifting subpulses. Individual emission of bright pulsar reveals the structure of single pulses which often consist of a number of subpulses. In some cases these subpulses demonstrate a more or less regular drift. This phenomenon manifests itself by a systematic change of phase in succesive pulses (e.g. Manchester et al. 1975, Rankin 1986). The subpulses drift slowly across the profile, forming the so called drift bands. The intensity of drifting subpulses is monotonically modulated along a drift band. The best studied pulsar with drifting subpulses is the PSR 0809+74 (Fig. 4).

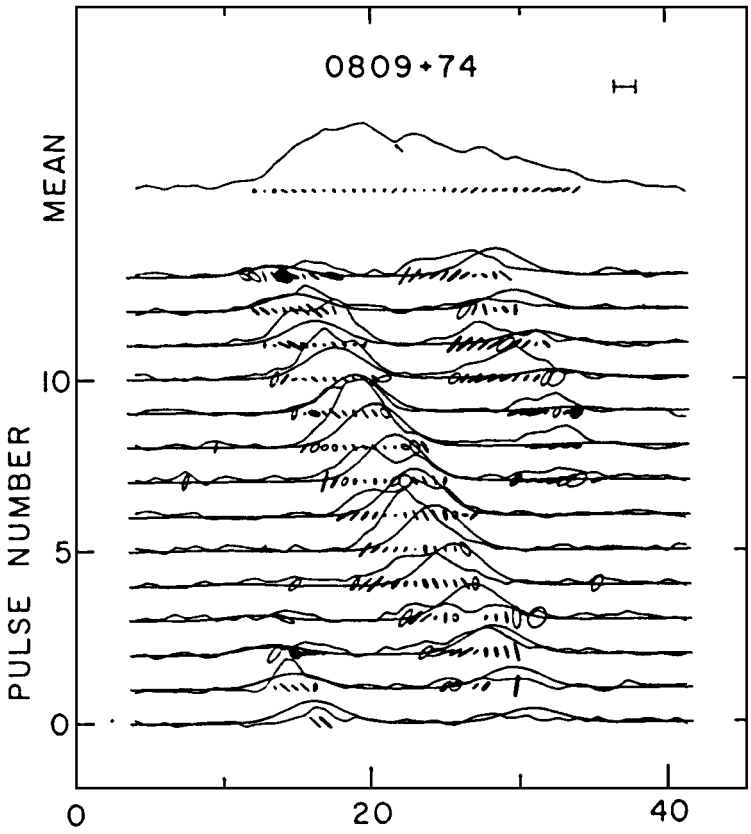

Fig. 4. Comparison of modelled and actual emission of PSR 0809+74 at 147 MHz (after Manchester et al. 1975, their Fig. 6a). The modelling includes only the total power modulation (smooth lines).

The most natural interpretation of drifting subpulses phenomenon is a slow rotation of the subpulse-associated plasma column around the symmetry axis (RS 1975, Gil et al. 1996), which for simplicity will be identified with the dipole moment axis here. As follows from considerations of section 2, the subpulse emission can be generated at the final stage of spark evolution, which feed the subpulse-associated plasma column above it. This stage lasts about $\Delta t/c$ and it takes about $\tau \sim \mathcal{R}/c$ to develope a spark from the vacuum to the "gap-emptying phase". Thus, in order to estimate the effective velocity

corresponding to the subpulse drift one has to multiply the drift velocity expressed in Eq. 13 by the factor $\Delta t/\tau \sim h/\mathcal{R}$. Then the linear rotation velocity of the (drifting) subpulse-associated plasma column can be expressed in the form

$$v_{ds} = \frac{h}{\mathcal{R}} \mathcal{F} c \Delta E / B_s \ \left[\frac{\mathrm{cm}}{\mathrm{s}}\right], \tag{23}$$

where

$$\Delta E = \frac{2\pi}{cP} \frac{B_s h^2}{r_p(1-s)}, \tag{24}$$

(RS 1975). Here B_s is the surface magnetic field, r_p is the Goldreich-Julian (1969) polar cap radius, h is the gap height (Eq. 1), $\mathcal{F}$ is the filling factor expressed by Eq. 12 and $0 \leq s \leq 1$ is the mapping parameter ($s = 0$ at the pole and $s = 1$ at the polar cap boundary).

The subpulse-associated plasma column completes one rotation in a time interval

$$\hat{P}_3 = \frac{2\pi s r_p}{v_{ds}} = \frac{r_p^2 \mathcal{R} s(1-s)}{h^3 \mathcal{F}} P = \frac{\mathcal{R}}{h} \frac{s(s-1)}{\mathcal{F}} a^2 P, \tag{25}$$

where $a \approx r_p/h$ (Eq. 2). Thus, the vertical distance between the driftbands is $P_3 = \hat{P}_3/N_s$ (Fig. 4), where N_s is the number of sparks circulating at a distance $d = s \cdot r_p$ from the pole. We can now calculate the so called drift rate

$$\mathcal{D} = \frac{P}{\hat{P}_3} 360^\circ = \frac{h \mathcal{F} 360^\circ}{\mathcal{R} s(s-1) a^2}, \tag{26}$$

which describes the rate of circular drift motion of subpulse-associated plasma columns expressed in degrees per pulsar period P.

We have modelled the radio emission of the PSR 0809+74, using a technique developed in Gil et al. 1995 and Gil and Krawczyk 1996. The results of modelling are compared with the actual modulation pattern of PSR 0809+74 in Fig. 4. The modelling procedure gives $n = \frac{1}{2}a = 2$ (Eqs. 1 and 14) and the drift rate $\mathcal{D}_m \approx 4^\circ$ per period $P = 1.29$ s. This means that the drifting subpulses in PSR 0809+74 correspond to the second ring of sparks circulating on the polar cap at $s \approx 0.8$. Since $a = r_p/h = 4$ then from Eq. 2 we obtain $\mathcal{R}_6 = 0.02$ or $\mathcal{R} = 2 \cdot 10^4$ cm ($\dot{P} = 1.7 \cdot 10^{-16}$) and from Eq. 12 we obtain $\mathcal{F} = 0.25$. Assuming that $B_s = B_{12} \cdot 10^{12}$ G, where $B_{12} = 3.2 \cdot 10^7 (P\dot{P})^{1/2} = 0.47$ one obtains from Eq. 1 that $h = 2.76 \cdot 10^3$ cm and $h/\mathcal{R} = 0.14$. Putting the above quantities into the Eq. 26 one gets $\mathcal{D} = 4.8^\circ$, very close to $\mathcal{D}_m = 4^\circ$ adopted in the modelling procedure (Fig. 4). Moreover, the location of PSR 0809+74 on the $P - \dot{P}$ diagram (thick cross in Fig. 1) corresponds exactly to $\mathcal{R}_6 = 0.02$ provided that $a = 4$. These facts are not trivial and demonstrate high degree of self-consistency of our model.

Finally, we can refer to the Eq. 19, which describes the location of pulsar radio emission region. The succesful modelling procedure leading to the Fig. 4 requires the emission altitude $r = 45 \cdot R$. Thus, for $P = 1.3$ s, $B_{12} = 0.47$ and $\mathcal{R}_6 = 0.02$ one obtains the Lorentz factor of the secondary plasma $\gamma_p \approx 85$, in consistency with an independent arguments based on the physics of the Sturrock's reproduction process (Gil et al. 1996).

5. Summary. In this paper we propose the pulsar model, which seems to offer a natural explanation of all phenomena observed in pulsar radiation. The proposed model is

self-consistent and based upon a few simple and natural assumptions. It relates conditions for the coherent radio emission in the lower magnetosphere with phenomena occurring within the polar gap, where a very high potential drop $\Delta V \geq 10^{12}$ V developes. We argue that the morphological pulsar properties (Rankin 1983, 1990, 1992, 1993, Gil et al. 1993a) are consistent with the non-stationary gap, in which the unipolar potential drop is discharged via a number of sparks (RS 1975). We estimated that both the characteristic dimension of sparks, as well as a distance between them is approximately equal to the RS polar gap height $h \sim 10^3$ cm. The sparks develop on dynamical time scale of the order of 10 microseconds, after which they reappear at approximately the same place due to intense thermo-emission caused by the back streaming electrons heating the base of the spark on the polar cap surface. One spark operates at the local surface magnetic pole and other sparks perform more or less ordered circumferential motion around the pole. Such an organization of the polar cap results in a core/multiconal structure of the mean pulsar beam, evidence of which was clearly demonstrated by several authors (Rankin 1983, 1990, 1992, 1993, Gil et al. 1993b). The observed number of profile components $N \leq a + 1$ (Eq. 15) is apparently smaller than 9. This explains why pulsars with complex profiles (cT, Q and M) occupy regions of small $a \approx r_p/h < 10$ (Eq. 2) on the $P - \dot{P}$ diagram. Moreover, pulsars with drifting subpulses also appear in regions of small a (crosses in Fig. 1). Obviously, drifting subpulses can be observed in pulsars which show subpulses in their single pulse emission in the first place. Within our model this is possible only if $a < 10$. On the other hand, simple and amorphous (with no hints of subpulse modulation) profiles require large values of $a > 10$. These pulsars are apparently separated from those with complex profiles on the $P - \dot{P}$ diagram (stars in Fig. 1).

The physical processes leading to the sparking avalanche development require that the surface magnetic field has relatively low radius of curvature $\mathcal{R} < 10^6$ cm. We argue that the best candidate for the surface magnetic structure is a sunspot like magnetic field. Evidence for such surface magnetic field has already been presented on both theoretical (Ruderman 1991 a,b,c) and observational (Page and Sarmiento 1996, Bulik et al. 1992) grounds.

The spark avalanche develops rapidly during $\tau \sim \mathcal{R}/c$, increasing exponentially the number density of the produced electrons and positrons. When the number density reaches the Goldreich-Julian (1969) corotational value, the spark terminates via a short gap-emptying phase of duration about h/c. This is a time interval separating two consecutive sparks. When the surface magnetic field has a sunspot like structure, the electrons and positrons accelerated within the gap always flow along closed magnetic field lines, despite the open dipolar field lines determining the polar cap region. It is worth stressing that this solves the long standing "current closure" problem. In fact, the charged particles within the gap never reach the open dipolar field lines. However, the high energy curvature photons emitted by positrons moving relativistically along closed lines within the accelerating gap reach the regions above the polar gap, where the radius of curvature of magnetic field lines is still suitable to produce additional electron-positron pair via the so-called Sturrock multiplication process (RS, Sturrock 1971). Since the potential drop in this region is negligible, the very high density $n_p = \chi_p \cdot n_{_{GJ}}$ secondary plasma originates, where the multiplication factor $\chi_p \sim 10^4$. The kinetic energy of this plasma is extracted

from the polar gap via the curvature gamma photons. Since the maximum Lorentz factor within the gap is about 10^6, it is obvious that the Lorentz factor of the bulk of secondary plasma $\gamma \leq 100$. However, one should expect a large thermal spread $\Delta\gamma \sim \gamma$, with the tail values of γ up to a few hundreds.

Two clouds of the secondary plasma corresponding to the two consecutive sparks are separated in time by about h/c. The bulk of the secondary plasma of the previous spark is penetrated by the beam of faster plasma particles corresponding to the high energy tail of the distribution function of the secondary plasma associated with the next spark. This excites the Langmuir waves in the secondary plasma (the same beam-plasma penetration applies to any pair of consecutive sparks). The amplitude of electrostatic oscillations associated with Langmuir waves is high enough to cause their non-linear evolution due to the modulational instability. As a result the soliton with a net charge is formed, which moves relativistically along curved dipolar magnetic field lines with a Lorentz factor corresponding to the resonant particles of the beam. Due to this motion the coherent curvature radio emission is generated, with polarization properties similar to that of a single particle curvature radiation. The altitude at which the solitons can be formed agrees well with other emission altitude estimates (e.g. Cordes 1992), including the one obtained by the method of first order relativistic corrections to the curvature radiation polarization characteristics (Blaskiewicz et al. 1991). It is argued that one soliton can easily radiate as much as 10^{21} erg/s, which for all available solitons gives a power of about $10^{23} - 10^{28}$ erg/s. This is just a typical range of pulsar radio luminosities.

References

J. Arons, 1981, *ApJ*, 248, 1099.
J. Arons, 1992, *Proc. of the IAU Colloq. 128*, ed. Hankins, T.H., Rankin, J.M., and Gil, J., p.56.
E. Asséo, R. Pellat and M. Rosado, 1980, *ApJ*, 239, 661.
E. Asséo, R. Pellat and H. Sol, 1983, *ApJ*, 266, 201.
G. Benford and R. Buschauer, 1977, *MNRAS*, 179, 189.
C.-I. Björnsson, 1996, *ApJ*, in press.
M. Blaskiewicz, J. M. Cordes and I. Waserman, 1991, *ApJ*, 370, 643.
T. Bulik, P. Meszaros, J. W. Woo, F. Nagase and K. Makishime, 1992, *ApJ*, 395, 564.
A. F. Cheng and M. A. Ruderman, 1977, *ApJ*, 214, 598.
A. F. Cheng and M. A. Ruderman, 1980, *ApJ*, 235, 576.
J. M. Cordes, 1992, *Proc. of the IAU Colloq. 128*, ed. Hankins, T.H., Rankin, J.M., and Gil, J., p.253.
V. D. Egorenkov, J. G. Lominadze and P. G. Mamradze, 1983, *Astrofizika*, 19, 753.
T. Erber, 1966, *Rev. Mod. Phys.*, 38, 626.
A. A. Galeev and R. Z. Sagdeev, 1973, *Rev. Plasma Phys.*, ed. Leontovich M.A., vol.7, Moscow.
J. Gil and J. K. Snakowski, 1990a, *A&A*, 234, 237.
J. Gil and J. K. Snakowski, J.K, 1990b, *A&A*, 234, 269.
J. Gil, 1992, *A&A*, 256, 495.

J. A. Gil, J. Kijak and P. Życki, 1993a, *A&A*, 272, 207.
J. A. Gil, J. Kijak and J. H. Seiradakis, 1993b, *A&A*, 272, 268.
J. Gil, J. Kijak, O. Maron and M. Sendyk, 1995, *A&A*, 301, 177.
J. Gil and A. G. Lyne, 1995, *MNRAS*, 276, L55.
J. Gil and A. Krawczyk, 1996a, *MNRAS*, 280, 143.
J. Gil and A. Krawczyk, 1996b, *MNRAS*, submitted.
J. Gil, G. I. Melikidze and A. D. Pataraya, 1996, in preparation.
P. Goldreich and H. Julian, 1969, *ApJ*, 157, 869.
D. M. Gould, 1994, PhD Thesis, University of Manchester, Dept. of Physics.
Y. H. Ichikawa, T. Suzuki and T. Taniuti, 1973, *J. Phys. Soc. Japan*, 34, 1089.
V. I. Karpman, C. A. Norman, D. ter Haar and V. N. Tsitovich, 1975 *Physics Scripta*, 11, 271.
A. Z. Kazbegi, G. Z. Machabeli, G. I. Melikidze and V. V. Usov, 1988, *Proc. of the Joint Varenna-Abastumani International School and Workshop on Plasma Astrophysics*, ed. T.D. Guyenne, ESA SP-285, Vol. I (Paris: European Space Agency), p.271.
A. Z. Kazbegi, G. Z. Machabeli and G. I. Melikidze, 1992, *Proc. of the IAU Colloq. 128*, ed. Hankins, T.H., Rankin, J.M. and Gil, J., p.232.
N. A. Krall, A. W. Tripolpiece, 1973, *Principles of Plasma Physics*, Mc-Graw Hill
J. G. Lominadze, G. Z. Machabeli, G. I. Melikidze and A. D. Pataraya, 1986, *Sov. J. Plasma Phys.*, 12, 712.
G. Z. Machabeli, 1991, Plasma Phys. and Controlled Fusion, 33, 1227.
R. N. Manchester, J. H. Taylor and G. R. Huguenin, 1975, *ApJ*, 196, 83-102.
R. N. Manchester and J. H. Taylor, 1977, *Pulsars*, Freeman, San Francisco.
R. N. Manchester and S. Johnston, 1995, *ApJ*, 441, L65.
G. I. Melikidze and A. D. Pataraya, 1984, *Astrofizika*, 20, 157.
D. B. Melrose, 1995, *J.Astrophys.Astr.*, 16, 137.
D. Page and A. Sarmiento, 1996, *ApJ*, in press.
V. Radhakrishnan and D. J. Cooke, 1969, *Astrophys. Lett.*, 3, 225.
J. M. Rankin, 1983, *ApJ*, 274, 333.
J. M. Rankin, 1986, *ApJ*, 301, 901.
J. M. Rankin, 1990, *ApJ*, 352, 314.
J. M. Rankin, 1992, *Proceedings of IAU Colloquimum 128*, ed. Hankins, T.H., Rankin, J.M. and Gil, J.A., p.133.
J. M. Rankin, 1993, *ApJ*, 405, 285.
M. A. Ruderman and P. G. Sutherland, 1975, *ApJ* 196, 51 (RS).
M. A. Ruderman, 1991a, *ApJ*, 366, 261.
M. A. Ruderman, 1991b, *ApJ*, 382, 576.
M. A. Ruderman, 1991c, *ApJ*, 382, 587.
P. A. Sturrock, 1971, *ApJ*, 164, 529.
V. V. Usov, 1987, *ApJ*, 320, 333.